Molecular Cell, Volume *46*

Supplemental Information

Mechanism of Translesion Transcription by RNA Polymerase II and Its Role in Cellular Resistance to DNA Damage

Celine Walmacq, Alan C.M. Cheung, Maria L. Kireeva, Lucyna Lubkowska, Chengcheng Ye, Deanna Gotte, Jeffrey N. Strathern, Thomas Carell, Patrick Cramer, and Mikhail Kashlev

Supplemental Text

1. Elongation Rate of WT, Rpb1-E1103G, Rpb1-T1095G, and Rpb1-G730D Pol II Mutants

We determined the bulk elongation rates for TECs by WT Pol II and E1103G, T1095G and G730D mutants (Domecq et al., 2010); Supplemental Table S1). At 10 μM NTPs, the WT Pol II exhibits a slow elongation rate with the major pausing and arrest at the U21 and U27 positions. At 200 μM NTP, the elongation rate increased about ten-fold and all pauses decreased or disappeared (Fig. S1A). Rpb1-E1103G and Rpb1-T1095G mutants showed a 3-fold and 2-fold increase of the bulk rate compared to the WT, respectively (Fig.S1A, compare lanes 6, 24 and 8, 17). These results were consistent with the previously reported biochemical phenotype of Rpb1-E1103G mutation (Kaplan et al., 2008; Kireeva et al., 2008; Malagon et al., 2006) and with the expected property of Rpb1-T1095G mutation localized in the same biochemical pathway governing the trigger loop mobility. Similar to E1103G substitution, T1095G was proposed to promote closure of the trigger loop (Kireeva et al., 2008). In contrast, Rpb1-G730D mutation conferred a severe >10-fold decrease of the elongation rate and induced a prolonged pausing at U21 and U27 positions at both NTP concentrations (lanes 8 and 40). The altered catalytic activity of these mutants was further confirmed by pre-steady states kinetic analysis of a single NTP addition (data not shown). The positive correlation between the increased catalytic activity and the efficient TLS suggests that the rate of chemistry may represent a limiting step during TLS, which is also consistent with the dramatically decreased TLS observed for the slow Rpb1-G730D Pol II. On the other hand, a relationship between the TLS and fidelity was clearly dependent on the location of the mutations (Fig.1A).

2. NTP Competition Assay for Transcription Fidelity

Transcription fidelity parameter reflects the ability of Pol II to select a correct NTP out of pool of 4 NTPs simultaneously present in the reaction. Fidelity depends on the apparent maximal polymerization rate constant (k_{pol}) and the apparent affinity of the polymerase to the substrate NTP (K_D). Fidelity is quantified as $(k_{pol}/K_D)^{\text{cognate NTP}}/ (k_{pol}/K_D)^{\text{mismatched NTP}}$, with k_{pol} and K_D for the cognate and the mismatched substrates NTP obtained from the [NTP] dependence of the apparent NMP incorporation rate constants (Kireeva et al., 2008). Although being highly reliable, this approach is laborious; in addition, the precision of the fidelity quantification is relatively low because the errors of each out of the four parameters used for its quantification are accumulated. Here, we present an alternative technique for rapid evaluation of transcription fidelity in a reaction containing both correct and incorrect NTP substrates that compete for binding to the active center. The misincorporation products are easily identified by their altered mobility in the urea-PAGE compared to the regular products (Fig. S1B). In this assay, the fidelity parameter for the WT Pol II and its mutant variants is calculated from the yields of the normal and the misincorporated RNAs accumulated in the same sample after normalization for difference in the substrate concentrations

as described below. The NTP competition assay produces matching fidelity parameters with the conventional NTP titration assay (Fig. S1B, graph on the top).

Briefly, WT and E1103G Pol II TECs were assembled *in vitro* using 9-nt RNA (TEC9) with 45-nt template coding for GMP, AMP and CMP at the + 10, 11 and 12 positions of the transcript (G_{10}, A_{11}, and C_{12}, respectively; Fig. S1B; Supplemental Table S2). Incubation of TEC9 with a mixture of the cognate GTP and the non-cognate ATP (the preferred misincorporation substrate for G_{10} position) leads to AMP misincorporation for GMP (A^*_{10}) competing with a proper incorporation of GMP (G_{10}). AMP is also accurately incorporated at the next A_{11} position to form $A^*_{10}A_{11}$ product along with the accurate $G_{10}A_{11}$ RNA (Fig. S1B, lanes 4-7; 11-14). The latter product is also partially extended by misincorporation of AMP for CMP at the + 12 position ($G_{10}A_{11}A^*_{12}$). We calculated the GMP incorporation fidelity for each GTP/ATP ratio as the (% correct incorporation × [ATP]) / (% incorrect incorporation × [GTP]). The GMP incorporation fidelity was equal to 0.9×10^5 and 0.3×10^5 for the WT and E1103G mutant, respectively (~1 error for 90,000 and 30,000 additions at equal ATP and GTP concentrations). Thus, the fidelity of E1103G mutant was 3 times lower than that of the WT Pol II for G_{10} position. Importantly, the magnitude of the fidelity defect in the E1103G mutant was in a good agreement with our previous work employing the standard technique (Kireeva et al., 2008). In this assay, T1095G and G730D enzymes exhibited ~2-fold and ~3.5-fold decrease of transcription fidelity, respectively (Fig. S1B, graph at the bottom).

To further validate the NTP competition assay, we determined fidelity at the same G_{10} position as a conventional k_{pol}/K_D ratio for the WT and E1103G Pol II as described previously (Kireeva et al., 2011). The incorporation rates for the correct and the incorrect NTP were defined over a 0.01-0.5 mM range of GTP and a 0.1-2 mM range of ATP and plotted against the substrate concentration (data not shown). The maximum polymerization rate, k_{pol}, and the dissociation constant, K_D, were obtained from the resulting data by a non-linear fit using the following equation $k= k_{pol} \times [NTP]/ (K_D + NTP)$. The fidelity parameter was determined by dividing k_{pol}/K_D for the correct GTP and k_{pol}/K_D for the incorrect ATP (Kireeva et al., 2008; Walmacq et al., 2009). The graphs on the right side of Figure S1B show that both assays produced the matching results for the WT Pol II and E1103G mutant.

3. E1103/T1095 and G730 Residues Localize to Separate Domains near Pol II Active Center

Rpb1-E1103 residue is located at the base of the trigger loop, a flexible element of the catalytic Rpb1 subunit closing on the active center after binding of NTP substrate (Vassylyev et al., 2007; Wang et al., 2006). In the opened conformation of the loop, T1095 residue is positioned in a close proximity to the E1103 residue (Fig. S1C). Upon closure of the loop, T1095 moves at a large distance toward the polymerase active center, and the E1103-T1095 interaction becomes broken. As we proposed previously (Kireeva et al., 2008; Walmacq et al., 2009), the interaction between T1095 and E1103 might stabilize the

opened state of the active center, facilitating the release of a non-cognate NTP before catalysis resulting in the improved fidelity (Fig. S1C). Our observation that Rpb1-T1095G mutation conferred a significant fidelity defect *in vitro* supported this hypothesis. Note, that in the closed trigger loop configuration, T1095 is located at a shorter distance from the active center than E1103, which cannot explain the stronger effect of E1103G mutation on fidelity. Most likely, E1103 residue has an additional function in fidelity control distinct from its role in the trigger loop mobilization.

Rpb1-G730D mutation substantially compromised transcription fidelity *in vitro* as was revealed by the NTP competition assay for the G_{10} position (Fig. S1B). G730 residue is embedded in the secondary channel of Pol II at a short distance from the active center. It localizes to the tip of a long α21/22-helix bundle connecting the active center with a rim of the secondary channel. G730 makes an interface between α21 helix of the bundle and short α22/23 helices forming a part of the active center. A hinge between the α22/23 helices contains an evolutionary conservative K752 residue directly contacting the β and γ phosphate of the incoming NTP in the active center. It has been proposed that K752 participates in an alignment of the β/γ phosphate moiety of the NTP with the 3' OH group in the RNA to facilitate the catalysis (Kireeva et al., 2009; Xiong and Burton, 2007). Our preliminary data (manuscript in preparation) strongly indicated that the fidelity defect conferred by G730D mutation was due to the decreased rate of the correct NTP incorporation with a much smaller effect on the incorrect NTP, which resulted in low fidelity. This property was opposite to the nature of fidelity defect in E1103G/T1095G mutants where the rate of misincorporation was increased to the larger proportion compared to the normal incorporation rate. This difference suggested that the Rpb1 domains harboring G730 and E1103/T1095 residues control fidelity by different mechanisms. However, we cannot entirely exclude the possibility that the bulky G730D substitution might reduce fidelity by direct effect on the trigger loop mobility. Indeed, the α21/22-helix bundle carrying G730 forms a surface along which the trigger loop slides during its closure on the active center.

In summary, transcriptional fidelity of Pol II appears highly complex as both slow and fast Pol II mutant proteins exhibit severe fidelity defects. Our data demonstrate that for some Pol II mutants, there is a correlation between low-fidelity and lesion bypass efficiency as observed for E1103G and T1095G mutants, while for the low fidelity G730D mutant the mechanism responsible the low CPD bypass may be more related to the low catalytic activity of the enzyme leading to the failure in TLS. This notion is supported by the very slow rate of ATP addition against both thymidines of the CPD exhibited by WT Pol II, which indicated that catalysis represents a rate-limiting step during TLS.

4. The Opposite Phenotypes of Rpb1- G730D Mutation In Vivo and In Vitro

Rpb1-G730D mutation was initially isolated by Koyama and co-workers as a suppressor of the hypersensitivity to the oxidative stress of the yeast strains harboring deletions of RPB9 and DST1 genes coding for Pol II Rpb9 subunit and transcript cleavage factor TFIIS respectively (Koyama et al., 2010). Rpb9 and TFIIS have been shown to improve fidelity of transcription *in vitro* and *in vivo* (Koyama et al., 2003; Koyama et al., 2010; Walmacq et al., 2009). An oxidative stress causes accumulation of 8-oxoguanine in the cell leading to mis-incorporation of 8-oxoGMP for UMP and GMP by Pol II (Taddei et al., 1997). Using a genetic assay based on suppression of internal nonsense codon in an ORF of the reporter LacZ gene, this group showed that *rpb9*Δ and *dst1*Δ cells exhibited an elevated level of β-gal expression indicating transcription mis-reading of the LacZ internal stop codon *in vivo*. Rpb1-G730D mutation restored both the original low level of β-gal expression and oxidative stress sensitivity of *rpb9*Δ and *dst1*Δ cells (Koyama et al., 2010). However, the *in vivo* phenotype of rpb1-G730D mutation alone and the biochemical properties of the mutant enzyme have never been evaluated. Based solely on the *in vivo* results, the authors concluded that both effects of the G730D mutation were due to the intrinsically improved transcription fidelity.

We noted, that the *in vivo* system for isolation of G730D mutation relied on a specific type of Pol II infidelity involving misincorporation of 8-oxoguanine for GMP, which was different from misincorporation of AMP for GMP analyzed in the present work (Fig. S1B). However, our testing of Pol II fidelity in the similar sequence context and for similar types of misincorporation (8-oxoguanine for GTP) as the one used by Koyama and co-workers, showed that Rpb1-G730D enzyme exhibited the decreased fidelity for 8-oxoG misincorporation for GMP similar to the other types of misincorporation (data not shown). RNA polymerase II is a housekeeping enzyme and mutations in its catalytic Rpb1 subunit may have a global effect on transcriptome in yeast. The apparent inconsistency between the *in vivo* and *in vitro* results on Rpb1-G730D mutant could be explained by the indirect effect of the mutation on translational read through of the LacZ stop codon or on nonsense mediated mRNA decay pathway. This subject requires further investigation.

5. Making *rad16, rad26,* and *rad16rad26* Deletion Strains with Deficient GG-NER, TC-NER, and GG/TC-NER

The nucleotide excision repair pathway (NER) is the major pathway responsible for removing UV-induced CPD lesions. One of the distinctive features of NER is its variability in the rate of repair across the genome. On the one hand, the transcription-coupled DNA repair (TC-NER) recruits NER proteins to the actively transcribed genes resulting in a preferential repair of the transcribed DNA strand (Bohr et al., 1985; Mellon et al., 1987). The damages in the transcribed regions are preferentially recognized by presence of Pol II molecules stalled at the lesion. These molecules are used for initiation of transcription-

coupled DNA repair (Hanawalt and Spivak, 2008; Laine and Egly, 2006; Svejstrup, 2002). In a course of repair, Pol II is removed from the damage site by a proteolytic degradation or by restart of transcription after the lesion is repaired. The strand-specific removal of CPD lesions by TCR depends on the rad26 protein, the yeast counterpart of mammalian CSB (Guzder et al., 1996; van Gool et al., 1994). On the other hand, the global genomic repair (GG-NER) eliminates the DNA lesions in the non-transcribed strand or in silent genomic domains independently of transcription (Terleth et al., 1990; Verhage et al., 1994). In yeast, this pathway depends on *RAD7* and *RAD16* genes (Verhage et al., 1994), which are presumably involved in recognition of the lesion. Deletion of mammalian CSB gene results in severe TC-NER defects (Troelstra et al., 1992), increased sensitivity to UV light (Venema et al., 1990) and defect in recovery of total RNA synthesis following UV irradiation**.** In humans, defective TCR is associated with Cockayne syndrome (CS), a severe autosomal-recessive disorder characterized by UV sensitivity, premature aging, and progressive neurodevelopmental abnormality (Fousteri and Mullenders, 2008). In contrast to human CSB mutants, deletion of its yeast counterpart Rad26 has no effect on survival on yeast cells following UV irradiation unless the global genome repair is eliminated (van Gool et al., 1994). GG-NER repairs lesions in the transcribed strand in the absence of TC-NER (van Gool et al., 1994; Verhage et al., 1996). However, the mechanism by which the GG-NER proteins access the lesions in the template strand, which are protected by arrested Pol II, remains unknown. As a result, elimination of TC-NER does not lead to a detectable increase of cell sensitivity to UV light (van Gool et al., 1994) indicating that the very efficient GG-NER masks TC-NER. This *RAD16*-dependent compensatory mechanism hinders the analysis of the role of Pol II in TC-NER and in the other pathways leading to the UV resistance in yeast (Tijsterman et al., 1997; Verhage et al., 1996). Therefore, the elimination or reduction of the GG-NER is used as a versatile tool for study of the TC-NER related pathways. The mutants *rad7* and *rad16* have been used extensively to determine the specific contribution of TC-NER to damage removal in transcribed sequences (Li et al., 2006; Verhage et al., 1996).

To investigate the effect of Rpb1-E1103G and Rpb1-G730D mutations on the UV resistance, we first constructed yeast strains carrying *RPB1* gene on LEU2 plasmid in the *RAD16* and in the *rad16* deleted background and then analyzed their capacity to survive UV irradiation (Fig. S1A). After irradiation with increasing dose of UV, no enhancement of sensitivity to UV was observed in the *rpb1-E1103G* and *rpb1-G730D* mutants when compared to the wild-type cells (data not shown). As previously described, mutational inactivation of *RAD16* gene does not affect TC-NER but confers defect in GG-NER leading to partial sensitivity of yeast cells to UV irradiation (Verhage et al., 1994). The GG-NER attenuation in the *rad16* mutant revealed that Pol II directly contributes to the UV resistance (DNA damage tolerance) by activation of the lesion bypass pathway dependent on a conformational change in the active center of the enzyme. As mentioned above, Rad26 protein, the homolog of human CSB, is involved in initiation of TC-

NER and deletion of *RAD26* gene in yeast causes a strong inhibition of CPD repair in the transcribed DNA strand (Tijsterman and Brouwer, 1999; van Gool et al., 1994). As previously reported, deletion of *RAD26* gene in yeast only confers UV sensitivity when the *RAD16*-dependent pathway for global genome is eliminated (van Gool et al., 1994); compare *rad26* and r*ad1626* in Fig. 6B and Fig.S1D). The double deletion results in enhanced UV sensitivity above that conferred by *rad16* deletion alone. To evaluate a contribution of TLS to transcription-coupled repair, we constructed yeast strains harboring Pol II mutations with deficient global genomic repair (GG-NER) and/or transcription-coupled repair and assessed their UV survival rate (Fig.6B and Supplemental Experimental Procedures).

6. A CPD Lesion in the Template DNA Strand Strongly Interferes with Pol II Progression; the CPD in the Nontemplate Strand Does Not affect Pol II Transcription

The lesions of different chemical nature in the transcribed DNA strand typically obstruct transcription of prokaryotic and eukaryotic RNA polymerases (Donahue et al., 1994; Selby et al., 1997; Tornaletti et al., 1997; Tornaletti et al., 1999). The same lesions in the non-template strand, with the exception of the cisplatin adduct (Tornaletti et al., 2003) and non-B form DNA structures such as G4 quadruplexes (Tornaletti et al., 2008) have no effect. Our reconstitution system for TEC by yeast Pol II recapitulated these properties of the bulky CPD lesions initially observed in the complete promoter systems. The NTS-CPD (non-template) did not interfere with Pol II elongation (Fig. S1E, lanes 1-6 and 18-23) while the TS-CPD (template) completely stalled Pol II (lanes 7-12 and 24-29). Transcription was not affected until the 3' T of the TS-CPD has reached the polymerase active site. Pol II slowly incorporated NTP opposite the 3'T-CPD followed by an even slower incorporation opposite the 5'T-CPD (lanes 26-29). This pattern was consistent with previous reports (Brueckner et al., 2007). A low but detectable amount of a read through transcript was detected upon longer incubation time with high concentration of NTPs indicating the limited ability of Pol II to bypass CPD lesion in the template strand (lanes 28-29).

7. NTP Incorporation Opposite the 3'T and the 5'T- CPD for Rpb1-E1103G Pol II

We compared in detail a selectivity of NTP incorporation by the WT and the E1103G Pol II opposite the 3'T-CPD by incubation of TEC12 with individual NTPs. On undamaged templates, E1103G promoted different types of transcription errors incorporating U>G>C for ATP (Kireeva et al., 2008). Similarly, the mutation increased efficiency of the ATP insertion and misincorporation of GTP, CTP and UTP against the 3'T-CPD (Fig. S2A, lanes 2-5 and 9-12). Incubation of TEC12 with 4 NTPs revealed that the mutant Pol II also more readily incorporated the second ATP against the 5'T-CPD followed by escape from the lesion (lanes 6, 7 and 13, 14). In the presence of ATP alone, the mutant also showed the increased misincorporation of AMP for GMP one nucleotide downstream from the lesion (lanes 2 and 9).

TEC13, containing AMP incorporated against the 3'T-CPD was used to address the specificity of NTP incorporation against the 5'T-CPD (Fig. S2B, lane 2). E1103G mutation significantly increased the efficiency of cognate AMP incorporation without affecting UMP misincorporation (compare lanes 8-13 in Fig. 4A and lanes 5-10 in Fig. S2B). Misincorporation of GTP and CTP against the 5'T-CPD was not detected for both the WT and the mutant Pol II under these conditions (compare lanes 14-19 in Fig. 4A and lanes 11-16 in Fig. S2B). Notably, the mutant Pol II was not able to extend the 5'T-CPD:U14 mismatched derived from UMP misincorporation at the 5'T-CPD (lanes 8-10). This result was in a contrast to the increased efficiency of different types mismatch extension characteristic for the mutant on the non-damaged DNA (Kireeva et al., 2008). As it was observed for the WT enzyme, the U14 misincorporation by the mutant was significantly reduced in the presence of 4 NTPs compared to the UTP alone, indicating a competition between UTP and other NTPs (most likely ATP) for binding to the active center containing the 5'T-CPD base (Fig. S2B, lanes 4 and 8).

Figure S2C compares the parameters of the cognate ATP to the most structurally similar GTP incorporation against the 3'T-CPD for the WT and E1103G mutant. Note that this experiment involves a DNA/RNA scaffold different from the standard sequence used in this study (Fig. S2C, top panel). Similar to the regular template, the mutant Pol II incorporated the correct adenine opposite the 3'T-CPD 6-fold more rapidly than the WT enzyme. On the other hand, the mutation only moderately (<2-fold) increased the ATP incorporation against the corresponding base in the non-damaged DNA. The E1103G mutation also increased the rate of GTP mis-incorporation against the 3'T-CPD compared to the WT enzyme. However, the ability of the enzyme to discriminate between the correct ATP and the incorrect GTP at the 3'T-CPD was only slightly decreased by the mutation (Fig. S2C). Strikingly, the comparable rates of the ATP incorporation and GTP mis-incorporation observed in the single NTP assay did not lead to any detectable mis-incorporation of GTP against the 3'T-CPD during lesion bypass with 4 NTPs or with ATP+GTP (Fig. S2A, lanes 6, 7 and 13, 14; for A+G - data not shown). This result indicated that ATP was able to efficiently exchange with GTP in the active center before subsequent bond formation and the rate of exchange was not significantly altered by the E1103G mutation. Consequently, E1103G conferred an increase in the lesion bypass efficiency judged by the increased accumulation of the lesion bypass RO* product (Fig. 1C and Fig. S2A, compare lanes 6, 7 and 13, 14).

8. Rpb1-T1095G Promotes CPD Bypass Similar to Rpb1-E1103G Mutation

In the experiment of Fig. S1F, T1095G TEC12 stalled at the lesion was incubated with 1 mM NTPs to initiate the CPD bypass. T1095G Pol II negotiated the CPD barrier more efficiently than the WT Pol II (compare graphs in Fig. S1F and Fig. 1C). T1095G mutation promoted specifically ATP insertion opposite both thymines of the CPD and did not increase UTP misincorporation against the 5'T of the

CPD. This observation supports the model that interaction between T1095 and E1103 residues stabilizes the opened state of the trigger loop, which stimulates the lesion bypass. E1103 is located at a larger distance from the active center than T1095 residue (Fig. S1C). The reproducibly less efficient bypass by T1095G (~25%) compared to E1103G (~ 40%) mutant polymerases suggested that the E1103 residue additionally controls translesion synthesis by a mechanism distinct from the trigger loop mobilization. This mechanism may involve interaction of this residue with the bridge helix.

9. The Translesion Synthesis Strategy during DNA Transcription and Replication

Potential mechanism of low-fidelity nucleotide incorporation characteristic of translesion DNA polymerases (TLS) may be conserved to some extent with RNA polymerase II (Fig. S3). Translesion polymerases share the similar general architecture as the replicative DNA polymerases with a hand-like shape structure with palm, finger, and thumb domains forming the active site. The TLS have an additional domain 'PAD domain', which extends from the fingers to make extra contacts with DNA (Waters et al., 2009; Yang and Woodgate, 2007). TLS polymerases typically have an open grip on the DNA and manifests a reduced processivity compared to the replicative polymerases (Prakash et al., 2005; Waters et al., 2009). Importantly, translesion polymerases have a more spacious active site that allows accommodation of large bulky adducts and even two-covalently linked thymidine (Waters et al., 2009). TLS polymerases lack the intrinsic 3'->5' exonuclease domain of replicative polymerases, which is involved in proofreading. Occasionally, translesion synthesis can be beneficial. This is strikingly seen in the case of DNA Pol η, which is the primary TLS polymerase responsible in many organisms for error-free bypass of CPDs (Yang and Woodgate, 2007). *In vitro*, human and yeast Pol η incorporates correct adenines with identical efficiency opposite *cis-syn* TT dimers and non-dimerized thymines (Haracska et al., 2000; Masutani et al., 2000; Matsuda et al., 2000). Mutational inactivation of Pol η results in a cancer-prone genetic disorder xeroderma pigmentosum variant (XP-V), characterized by an increased incidence of skin-cancer and sensitivity to sunlight. The phenotype of Pol η deficiencies highlights its predominant role in the non-mutagenic bypass of CPD-lesions (Lehmann, 2005).

Based on these phenotypic and structural similarities, it is conceivable that RNA polymerase II, which has an intrinsic ability to bypass bulky adducts, switches to the mode structurally similar to the translesion DNA polymerase possessing low rate of NTP incorporation and increased flexibility of the active site facilitating accommodation of the lesion (Fig. S3, the top panel). When the damage is bypassed, RNA polymerase II switches back to the fast, highly processive and high fidelity mode. *Trans*-acting protein factors and *cis*-acting Pol II subunits may regulate the switch between the two modes. Indeed, Rpb9 subunit of Pol II has been shown to regulate mobility of the trigger loop similarly to the rpb1-E1103G mutation (Walmacq et al., 2009) and Rpb4/7 subunits to increase clamping of the template

DNA by the enzyme (Armache et al., 2003). Both these mechanisms may change the active site geometry and, consequently, the ability for TLS. Co-incidentally, Rpb4 and Rpb9 subunit have been shown to mediate the two separate pathways of TC-NER (Li and Smerdon, 2002).

S1

A

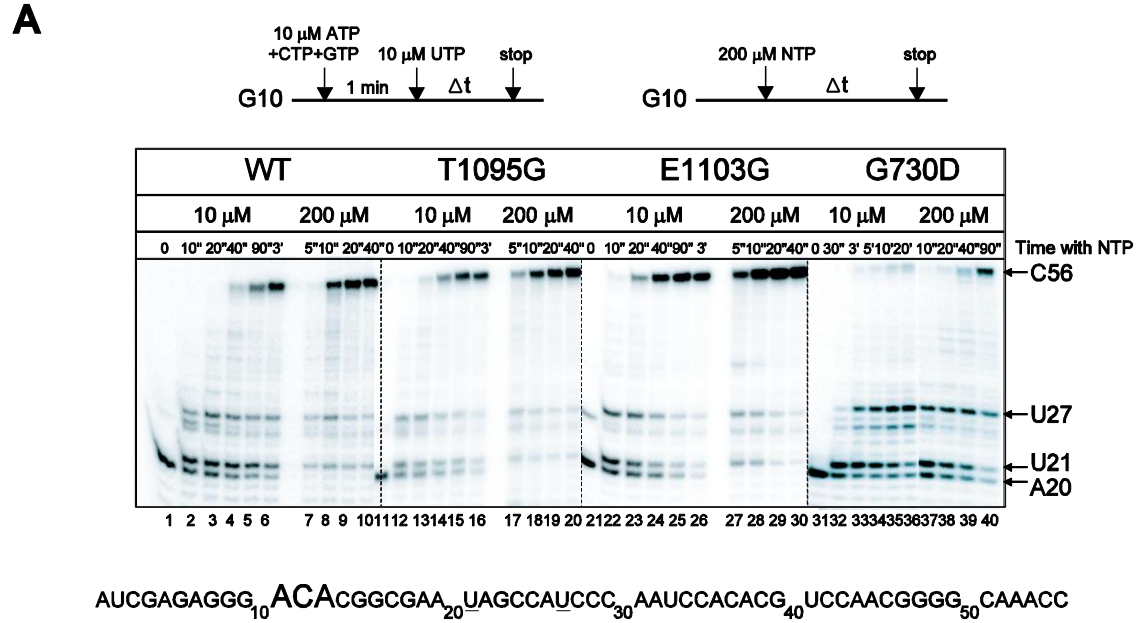
10 μM ATP
+CTP+GTP
10 μM UTP
stop
G10
1 min
Δt
200 μM NTP
stop
G10
Δt
WT
T1095G
E1103G
G730D
10 μM
200 μM
Time with NTP
C56
U27
U21
A20
AUCGAGAGGG10ACACGGCGAA20UAGCCAUCCC30AAUCCACACG40UCCAACGGGG50CAAACC

B

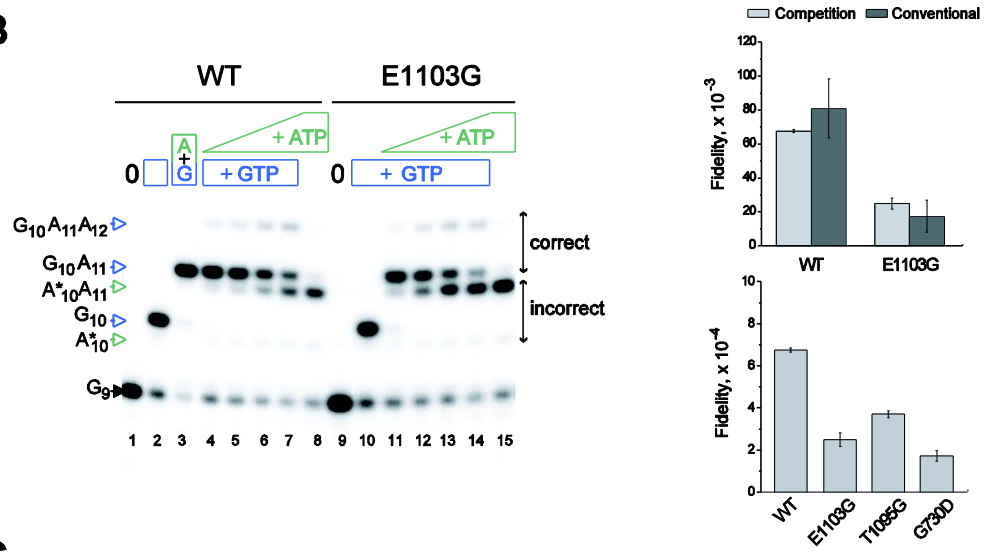
WT
E1103G
+ ATP
+ GTP
correct
incorrect
Competition
Conventional
Fidelity, x 10-3
Fidelity, x 10-4
WT
E1103G
T1095G
G730D

C

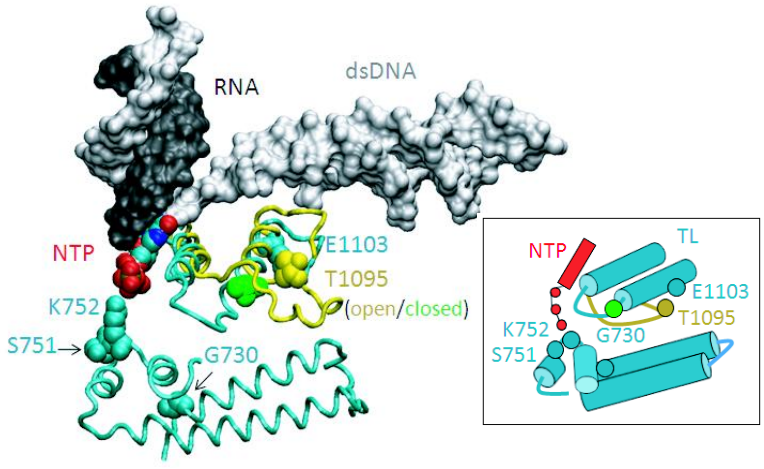
RNA
dsDNA
NTP
E1103
T1095
(open/closed)
K752
S751
G730
TL

Figure S1, Related to Figure 1.

(A) Transcription patterns of WT and Pol II mutants. The protocol is shown above the figure. TEC10 were assembled on D111 template as described in the Supplemental Experimental Procedures. TEC10 were either stalled at position A20 upstream from the U21 pause site followed by incubation with 10 μM NTPs or incubated with 200 μM NTPs for various times. The RNA sequence is shown at the bottom of the figure.

(B) Fidelity analysis of WT and Pol II mutants. Left panel: NTP competition assay for WT and error-prone E1103G Pol II mutant. E1103G TEC9 assembled on the 45-nt template with the 9-nt RNA was incubated simultaneously with the cognate GTP (20 nM; blue box) and the non-cognate ATP (green box) at various concentrations (0.1, 0.2, 0.5, 1 mM) for 3 min (WT) or 1 min (E1103G). As a control, TEC9 were also incubated with GTP only (lanes 2 and 10), GTP + ATP (10 μM each; lane 3) and ATP only (lanes 8 and 15). An accurate GMP incorporation at G_{10} position is discriminated from misincorporation of AMP (A^*_{10}, the asterisk indicates the misincorporation product) by the different mobility of the short RNAs in the gels. Blue arrows indicate the product of the cognate GMP incorporation and its subsequent extension to 11-nt and 12-nt by AMP incorporation ($G_{10}A_{11}$, $G_{10}A_{11}A_{12}$). Green arrows indicate the products of the non-cognate AMP incorporation and their subsequent extension by one nucleotide ($A^*_{10}A_{11}$). Lanes 1 and 9 correspond to the starting 9-nt RNA for WT and E1103G, respectively. Right panel: The conventional NTP titration and the NTP competition assays produce similar values for transcription fidelity. The plot represents an average of three experiments performed with different [GTP]/[ATP] ratios and the error bars indicate the standard deviation. The error-prone Rpb1-E1103G is the benchmark for the fidelity assay. Rpb1-T1095G and G730D mutants decrease transcription fidelity in the competition assay.

(C) Alignment of *S. cerevisiae* Pol II TEC structures. The structures [PDBs: 1Y1V (Kettenberger et al., 2004), yellow and 2E2H (Wang et al., 2006), cyan] depict the trigger loop in opened (yellow) and closed (cyan) conformations. Location of Thr1095 residue is shown for the opened and closed state of the trigger loop (shown in green color). The other structural elements are the same as in Fig. 1A. The inset shows schematic positions of the NTP in the active center (in red) and the two domains in Rpb1 subunit involved in control of transcription fidelity. The filled circles depict location of all Rpb1 mutations analyzed in this work. The opened position of the trigger loop is shown in yellow.

S1 (continued)

D

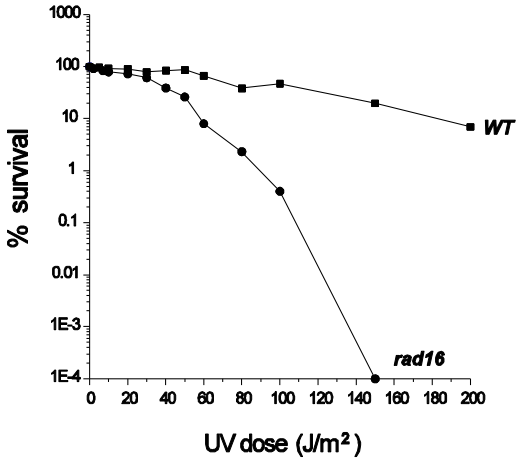

E

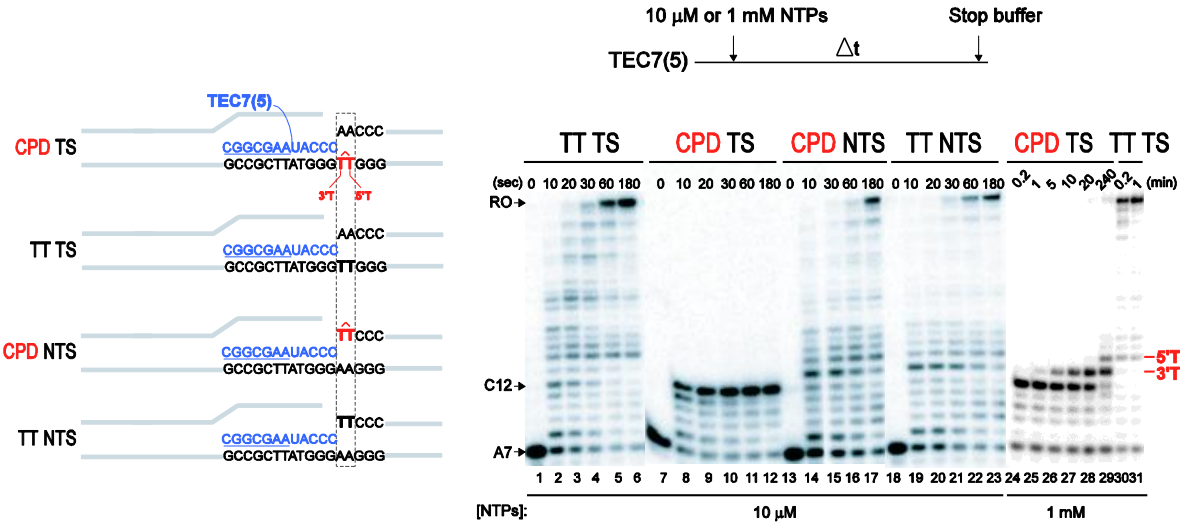

F

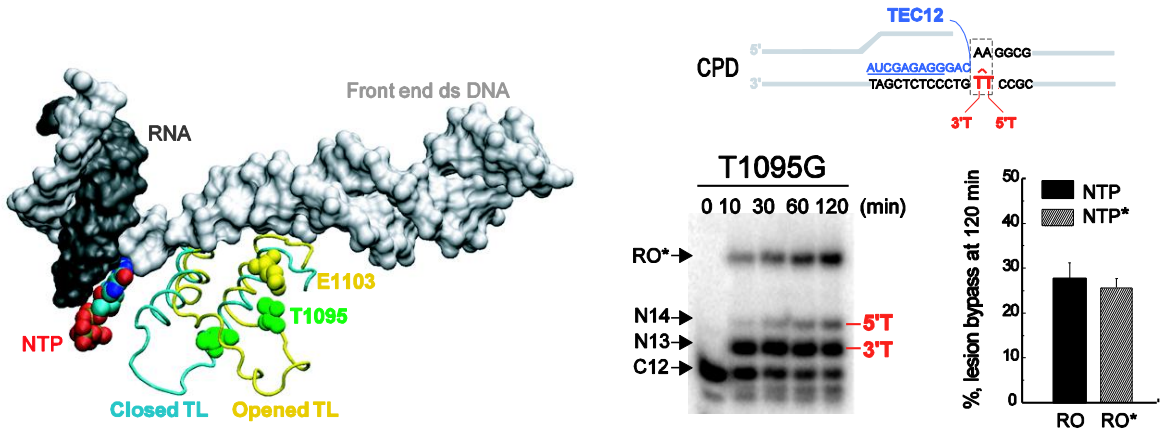

Figure S1 (continued), Related to Figure 1.

(D) UV survival curves for *RAD16* (MMTY102) and *rad16* (MMTY103) mutant. Cells were grown in YEPD, diluted in water, and irradiated with the indicated doses of UV, and dilutions were plated on YEPD. After 3 days of incubation at 28°C in the dark, colonies were counted and survival was calculated. *rad16* deletion confers partial cell UV sensitivity. Other conditions are the same as in the experiment of Fig. 1B.

(E) A CPD located in the template but not in the non-template strand arrests transcription. Left panel: Design of the templates. TEC7 was assembled on the 71-nt template and non-template DNA oligonucleotides (in gray) with the 5'-labeled RNA7 primer (shown in blue, underlined). The DNA oligonucleotides contained a CPD lesion (TT in red) in the template DNA strand (TS71-CPD25/NTS71-25) or in the non-template DNA strand (TS71-46/NTSCPD71-46) 5 nts downstream from the 3'end of the RNA7. The undamaged DNA was used as control for the corresponding CPD in the TS (TS71-CPD25/NTS71-25) or NTS strand (TS71-25B/NTS71-25B), respectively. Right panel: Time courses of extension of the RNA7 to the lesion at 10 μM (lanes 2-6, 8-12, 14-17, 19-23) and 1 mM (lanes 24-31) NTPs. Full-length transcript (RO, 51 nts) and the C12 RNA product of stalling in front of the TS-CPD are indicated. At low NTPs, Pol II transcribed to the site of the CPD lesion (C12), but not beyond. At 1 mM NTPs, Pol II slowly incorporated one nucleotide opposite the 3'T and 5'T of the CPD lesion (A13 and A14) followed by slow accumulation of the RO product, indicating a slow bypass of the lesion.

(F) Translesion synthesis by Rpb1-T1095G Pol II. The CPD-containing TEC12 was incubated with 1 mM ATP, GTP and UTP and chain-terminating 3'dCTP (100 μM) to facilitate detection of the lesion bypass product (RO*) derived from incorporation of 3'dCMP 3 nts downstream the lesion. The presence of terminating NTP did not affect the bypass efficiency compared to the standard chase with 4 NTPs (the graph of Fig. S1C). The other conditions are the same as in the experiment of Fig. 1C. The plot shows an average of the results of three experiments and the error bars indicate the standard deviation.

S2

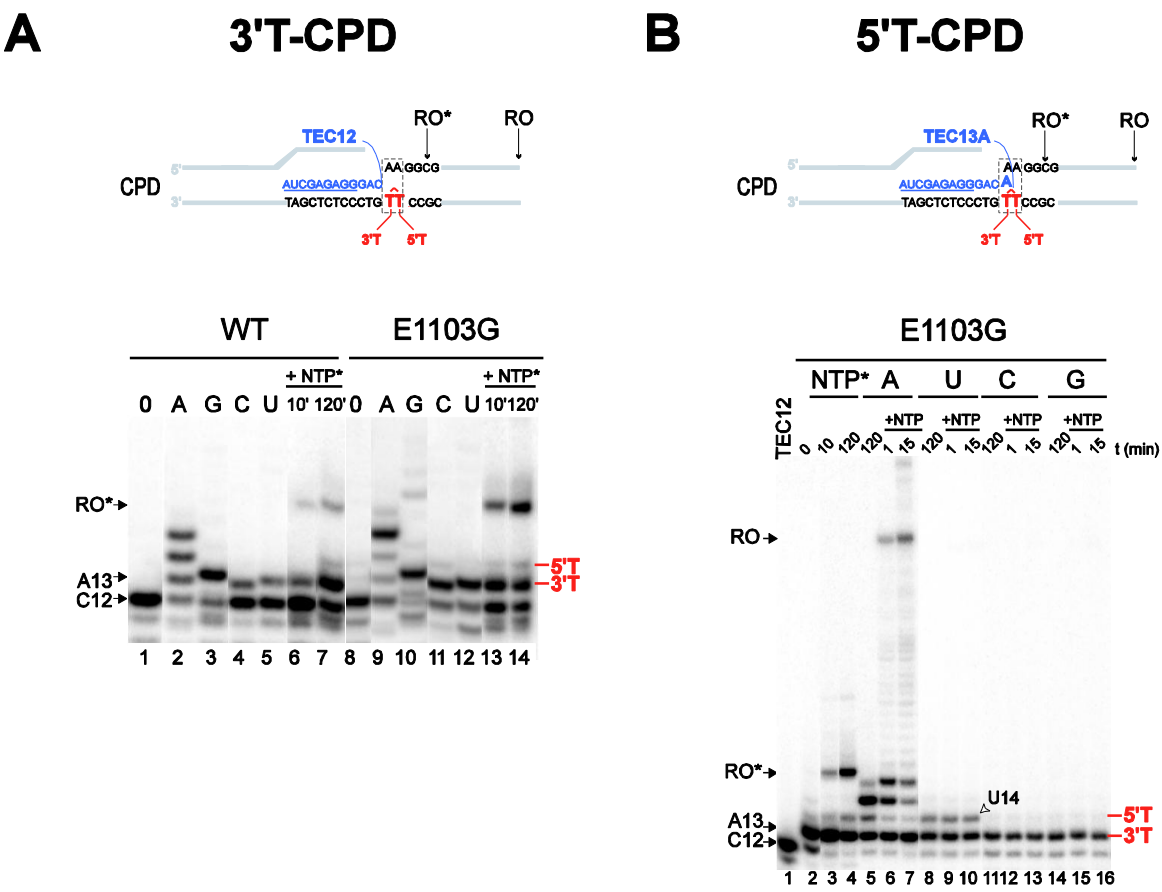

C

	WT		E1103G	
	TT k_{app} (s^{-1})	CPD k_{app} (s^{-1})	TT k_{app} (s^{-1})	CPD k_{app} (s^{-1})
ATP	107 ± 4	$(8.4 \pm 0.7)\times10^{-4}$	182 ± 7	$(54.8 \pm 3.5)\times10^{-4}$
GTP	$(3.9 \pm 0.3)\times10^{-4}$	$(3.4 \pm 0.2)\times10^{-4}$	$(34.3 \pm 3.2)\times10^{-4}$	$(23.8 \pm 2.2)\times10^{-4}$

Figure S2, Related to Figures 3A and 4A.

(A) Design of the templates. TEC12 was assembled on the templates NTS71-38/TS71-CPD38 and the 9-nt RNA (underlined). TEC12 was obtained by incubation with 5 μM GTP and ATP, followed by addition of CTP, washed and incubated with ATP, GTP, UTP and 3'dCTP mix (lanes 6, 7 and 13, 14) for 10 and 120 min. Alternatively, TEC12 was incubated with 1 mM of individual NTPs for 120 min (lanes 2-4 and 9-12). The distinct mobility of the 13-nt RNA products with different 3'-NMPs allowed detection of the mis-incorporation event at the 3'T-CPD in the reaction containing all 4 NTPs (lanes 2-5 and 6, 7 for the WT; lanes 9-12 and 13, 14 for the E1103G mutant). The uniform mobility of the 13-nt RNA product originated from transcription in the presence of all 4 NTPs clearly demonstrates lack of NTP mis-incorporation against the 3'T-CPD for both the WT and E1103G Pol II.

(B) Steps in translesion synthesis by error-prone E1103G Pol II. Pattern of the RNA extension opposite the 5'T-CPD by E1103G Pol II. The reaction conditions were the same as in the experiment of Fig. 3B. TEC13 mis-incorporated UTP, but not CTP or GTP against the 5'T-CPD (lanes 8-16). Incorporation of the cognate ATP (lane 5) led to an escape from the lesion upon addition of 4 NTPs for different amount of time (lanes 6, 7). Note, that 120-min incubation of TEC13 with 1 mM ATP promoted a substantial mis-incorporation of ATP for GTP one nucleotide downstream from the lesion (A15 product, lane 5). The majority of this product was chased after incubation with 4 NTPs (lanes 6, 7) illustrating the remarkable ability of the mutant Pol II to tolerate the mis-matched 3' RNA ends. This property additionally contributed to the increased lesion bypass by the mutant.

(C) Preferential AMP incorporation opposite the 3'T-CPD for the WT and E1103G Pol II mutant. Efficiency of the correct ATP and the incorrect GTP incorporation against the 3'T-CPD on the regular TT sequence and the CPD lesion by the WT and E1103G mutant (Template TS71-CPD25/NTS71-25/RNA7; sequence shown on the top and Table S1). The relative amount of the RNA extension products was quantified as described in Fig. 3C. The apparent rates for the cognate ATP and non-cognate GTP were obtained from single-exponential fit of three independent experimental data.

S3

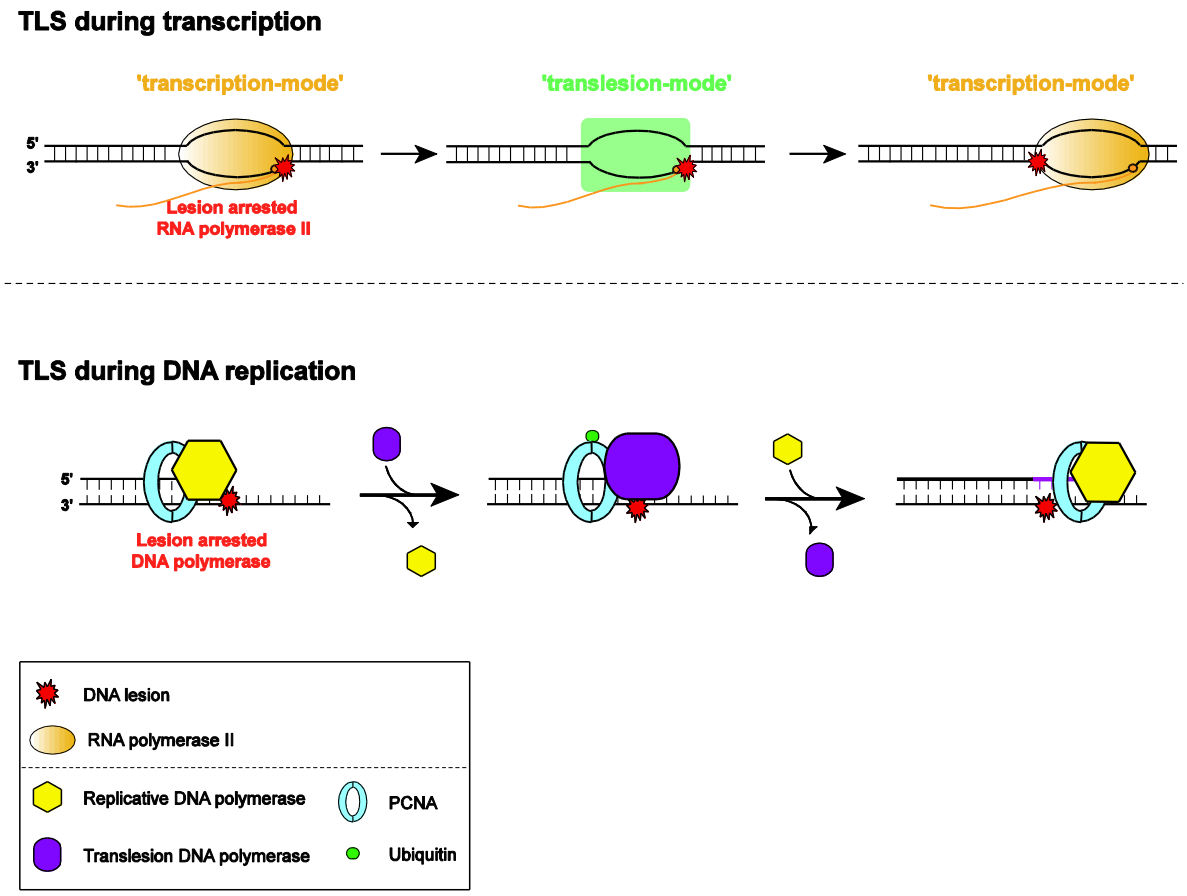

Figure S3, Related to Discussion. Translesion Synthesis by DNA and RNA Polymerases

The top picture: During TLS, RNA polymerase II switches to a 'translesion mode' characterized by a low efficiency of NTP incorporation, a low fidelity and a non-templated insertion opposite the 3'T-CPD. After lesion bypass, Pol II switches back to a 'transcription-mode' with a rapid templated NTP incorporation and a high fidelity. The switch between the two modes involves the *cis*-acting flexible elements in the rpb1 subunit [the trigger loop (1065-1112 a.a.), bridge helix (810-840 a.a.) and the 2-helix bundle (670-730 a.a.)] or putative trans-acting regulatory factors that might regulate lesion bypass efficiency *in vivo* (yet to be identified). The bottom picture: During TLS, high-fidelity replicative DNA polymerase is switched transiently to low-fidelity translesion DNA polymerase [adapted from (Waters et al., 2009)].

Table S1, Related to Experimental Procedures. Oligonucleotides Used for Transcription Assays, Exo III Footprinting, and Crystal Structure Analysis

Name	Sequence[a]
Biochemical Analysis Oligonucleotides	
RNA9	AUCGAGAGG
RNA7	CGGCGAA
NTS71-38	CCT ATA GGA TAC TTA CAG CCA TCG AGA GGG AC AA GG CGA ATA CCC ATC CCA ATC GGC CTG CTG GT GAC ACC
TS71-38	GGT GTC ACC AGC AGG CCG ATT GGG ATG GGT ATT CGC CTT GTC CCT CTC GAT GGC TGT AAG TAT CCT ATA GG
TS71CPD-38	GGT GTC ACC AGC AGG CCG ATT GGG ATG GGT ATT CGC C**TT** GTC CCT CTC GAT GGC TGT AAG TAT CCT ATA GG
NTS71-38B	CCT ATA GGA TAC TTA CAG CCA TCG AGA GGG AC TT GG CGA ATA CCC ATC CCA ATC GGC CTG CTG GT GAC ACC
TS71-38B	GGT GTC ACC AGC AGG CCG ATT GGG ATG GGT ATT CGC CAA GTC CCT CTC GAT GGC TGT AAG TAT CCT ATA GG
NTS71-25	CCT ATA GGA TAC TTA CAG CCA TCG AGA GGG ACA CGG CGA ATA CCC AAC CCA ATC GGC CTG CTG GT GAC ACC
TS71-25	GGT GTC ACC AGC AGG CCG ATT GGG TTG GGT ATT CGC CGT GTC CCT CTC GAT GGC TGT AAG TAT CCT ATA GG
NTS71-25B	CCT ATA GGA TAC TTA CAG CCA TCG AGA GGG ACA CGG CGA ATA CCC TTC CCA ATC GGC CTG CTG GT GAC ACC
TS71-25B	GGT GTC ACC AGC AGG CCG ATT GGG AAG GGT ATT CGC CGT GTC CCT CTC GAT GGC TGT AAG TAT CCT ATA GG
TS71CPD-25	GGT GTC ACC AGC AGG CCG ATT GGG **TT**G GGT ATT CGC CGT GTC CCT CTC GAT GGC TGT AAG TAT CCT ATA GG
NTS71-25E	CCT ATA GGA TAC TTA CAG CCA TCG AGA GGG ACA CGG CGA ATA CCC AAC CCA ATC GGC CTG CTG GT GAC ACC TGG
NTS71CPD-33	CCT ATA GGA TAC TTA CAG CCA TCG AGA GGG AC **TT** GG CGA ATA CCC ATC CCA ATC GGC CTG CTG GT GAC ACC
TS71-33	GGT GTC ACC AGC AGG CCG ATT GGG ATG GGT ATT CGC CAA GTC CCT CTC GAT GGC TGT AAG TAT CCT ATA GG
NTS71CPD-46	CCT ATA GGA TAC TTA CAG CCA TCG AGA GGG ACA CGG CGA ATA CCC **TT**C CCA ATC GGC CTG CTG GT GAC ACC
TS71-46	GGT GTC ACC AGC AGG CCG ATT GGG AAG GGT ATT CGC CGT GTC CCT CTC GAT GGC TGT AAG TAT CCT ATA GG
NTS71-25E2	ATA GGA TAC TTA CAG CCA TCG AGA GGG ACA CGG CGA ATA CCC AAC CCA ATC GGC CTG CTG GT GAC ACC
TS45	CTC TTT TCG CCT TGT CCC TCT CGA TGG CTG TAA GTA TCC TAT ACC
NTS45	GGT ATA GGA TAC TTA CAG CCA TCG AGA GGG ACA AGG CGA AAA GAG
TS-D111	GGT TTG CCC CGT TGG ACG TGT GGA TTG GGA TGG CTA TTC GCC GTG TCC CTC TCG ATG GCT GTA AGT ATC CTA TAG G
NTS-D111	CCT ATA GGA TAC TTA CAG CCA TCG AGA GGG ACA CGG CGA ATA GCC ATC CCA ATC CAC ACG TCC AAC GGG GCA AAC C
Crystal Structure Oligonucleotides	
Template-CPD	AGC TCA AGT ACT **TT**T TCC BGG TCA TT
Non-template	TAA GTA CTT GAG CT
RNA	UUC GAC CAG GAA

[a]Oligonucleotides sequences are presented 5'-3'. *Cis-syn* TT dimer are represented in red. B=5'bromo-uracil

Table S2, Related to Supplemental Experimental Procedures. Yeast Strains Used in This Study

Strains	Genotype
Strains used for Figures 1B and S1D*	
MMTY99 *RPB1*	*MATα his3Δ1 leu2Δ0 met15Δ0 ura3Δ0 rpb1::natMX can1-Δmush17-4 [pJS725 **URA3** RPB1]*
MMTY100 *rad16RPB1*	*MATα his3Δ1 leu2Δ0 met15Δ0 ura3Δ0 rpb1::natMX can1-Δmush17-4 rad16::kanMX [pJS725 **URA3** RPB1]*
MMTY102 *RPB1*	*MATα his3Δ1 leu2Δ0 met15Δ0 ura3Δ0 rpb1::natMX can1-Δmush17-4 [pJS757 **LEU2** RPB1]*
MMTY103 *rad16RPB1*	*MATα his3Δ1 leu2Δ0 met15Δ0 ura3Δ0 rpb1::natMX can1-Δmush17-4 rad16::kanMX [pJS757 **LEU2** RPB1]*
MMTY104 *rpb1-E1103G*	*MATα his3Δ1 leu2Δ0 met15Δ0 ura3Δ0 rpb1::natMX can1-Δmush17-4 [pJS781 **LEU2** rpb1-E1103G]*
MMTY105 *rad16rpb1-E1103G*	*MATα his3Δ1 leu2Δ0 met15Δ0 ura3Δ0 rpb1::natMX can1-Δmush17-4 rad16::kanMX [pJS781 **LEU2** rpb1-E1103G]*
MMTY106 *rpb1-G730D*	*MATα his3Δ1 leu2:ADH1prMBPA11 minus His3::kanMX met15Δ0 ura3Δ0 rpb1::kanMX [pCW01 **LEU2** rpb1-G730D]*
MMTY107 *rad16rpb1-G730D*	*MATα his3Δ1 leu2Δ0 met15Δ0 ura3Δ0 rpb1::natMX can1-Δmush17-4 rad16::kanMX [pCW01 **LEU2** rpb1-G730D]*
MMTY113 *rad26*	*MATa his3Δ1 leu2Δ0 met15Δ0 ura3Δ0 rad26::HyMX [pJS757 **LEU2** RPB1]*
Strains used for Figure 5C **	
MMTY115 *RPB1*[a]	*MATα his3Δ1 leu2Δ0 met15Δ0 ura3Δ0 rpb1::natMX can1-Δmush17-4 [pJS757 **LEU2** RPB1]*
MMTY116 *rad16RPB1*[a]	*MATa his3Δ1 leu2Δ0 met15Δ0 ura3Δ0 rpb1::natMX can1-Δmush17-4 rad16::kanMX [pJS757 **LEU2** RPB1]*
MMTY114 *rad26RPB1*[a]	*MATα his3Δ1 leu2Δ0 met15Δ0 ura3Δ0 rpb1::natMX can1-Δmush17-4 rad26::HyMX [pJS757 **LEU2** RPB1]*
MMT117 *rad16rad26RPB1*[a]	*MATa his3Δ1 leu2Δ0 met15Δ0 ura3Δ0 rpb1::natMX can1-Δmush17-4 rad16::kanMX rad26::HyMX [pJS757 **LEU2** RPB1]*
MMT119 *rpb1-E1103G*[b]	*MATa his3Δ1 leu2Δ0 met15Δ0 ura3Δ0 rpb1::natMX can1-Δmush17-4 [pJS781 **LEU2** rpb1-E1103G]*

MMTY120 *rad16rpb1-E1103G*[b]	*MATα his3Δ1 leu2Δ0 met15Δ0 ura3Δ0 rpb1::natMX can1-Δmush17-4 rad16::kanMX [pJS781* ***LEU2*** *rpb1-E1103G]*
MMTY118 *rad26rpb1-E1103G*[b]	*MATα his3Δ1 leu2Δ0 met15Δ0 ura3Δ0 rpb1::natMX can1-Δmush17-4 rad26::HyMX [pJS781* ***LEU2*** *rpb1-E1103G]*
MMTY121 *rad16rad26rpb1-E1103G*[b]	*MATa his3Δ1 leu2Δ0 met15Δ0 ura3Δ0 rpb1::natMX can1-Δmush17-4 rad16::kanMX rad26::HyMX [pJS781* ***LEU2*** *rpb1-E1103G]*
MMTY123 *rpb1-G730D*[c]	*MATα his3Δ1 leu2Δ0 met15Δ0 ura3Δ0 rpb1::natMX can1-Δmush17-4 [pCW01* ***LEU2*** *rpb1-G730D]*
MMTY124 *rad16rpb1-G730D*[c]	*MATα his3Δ1 leu2Δ0 met15Δ0 ura3Δ0 rpb1::natMX can1-Δmush17-4 rad16::kanMX [pCW01* ***LEU2*** *rpb1-G730D]*
MMTY122 *rad26rpb1-G730D*[c]	*MATa his3Δ1 leu2Δ0 met15Δ0 ura3Δ0 rpb1::natMX can1-Δmush17-4 rad26::HyMX [pCW01* ***LEU2*** *rpb1-G730D]*
MMTY125 *rad16rad26 rpb1-G730D*[c]	*MATα his3Δ1 leu2Δ0 met15Δ0 ura3Δ0 rpb1::natMX can1-Δmush17-4 rad16::kanMX rad26::HyMX [pCW01* ***LEU2*** *rpb1-G730D]*

***** Strains obtained by plasmid shuffle and used for Experiment described in Fig.1B and Suppl. Fig. S1D

****** Isogenic strains obtained from three different crosses a, b and c: (a) MMTY103 X MMTY113 (b) MMTY105 X MMTY113 (c) MMTY107 X MMTY113 and used for Experiment described in Figure 5C. Note that yeast strains obtained from plasmid shuffle (*) or from crosses (**) showed consistently comparable sensitivity to UV irradiation.

SUPPLEMENTAL EXPERIMENTAL PROCEDURES

Media, Yeast Manipulations, Strains

Media, growth conditions and yeast manipulations were as previously described (Malagon et al., 2006). All strains used are direct derivatives or closely related to the BY series of the yeast knockout collection into which we introduced different alleles of RPB1. Briefly, *rad16* strain from the BY collection (*MATa his3-Δ1 leu2-Δ0 met15-Δ0 ura3-Δ0 rad16::kanMX)* was crossed with MMTY99 (harboring the *RPB1* WT gene on *URA3* plasmid) and subjected to tetrad analysis. From the cross, the segregants were analyzed by G418 and 5-fluoroorotic acid treatments to identify haploids strains cells bearing *RPB1* gene in a *rad16* and *RAD16* genetic background. *RAD16 RPB1* (MMTY99) as well as *rad16 RPB1* (MMTY100) strains were then transformed with plasmids p*RPB1*, p*rpb1-E1103G*, p*rpb1-G730D* (*LEU2*). Subsequently, selection was performed in the presence of 5-fluoroorotic acid (Table S2,*). Yeast strains carrying *RPB1 WT*(MMTY103), *rpb1-E1103G* (MMTY105) or *rpb1-G730D* (MMTY107) mutation in the *rad16* background were crossed to *rad26* null mutant (MMTY13) to create *rad16rad26* double mutant (Table S2,**). From the cross, the segregants were scored by G418, hygromycine and 5-fluoroorotic acid treatments to identify haploids strains cells bearing *RPB1WT, rpb1-E1103G or rpb1-G730D* in various isogenic genetic backgrounds (*RAD16RAD26, rad16, rad26* and *rad16rad26)*. All yeast strain genotypes are described in Table S2.

Crystal Structure Analysis

Saccharomyces cerevisiae 12-subunit Pol II was prepared as described (Sydow et al., 2009). Purified Pol II was mixed with a fivefold molar excess of recombinant Rpb4/7 and twofold molar excess of a minimal nucleic acid scaffold (Table S1) prepared as described (Kettenberger et al., 2004) and incubated for 1 hr at 20°C before purification by gel filtration (Superose 6, GE healthcare) in Pol II buffer (5mM HEPES pH 7.0, 40mM ammonium sulfate, 10µM $ZnCl_2$ and 10mM DTT). The complex was concentrated to ~4mg/ml and additional nucleic acid scaffold added to a final concentration of 2µM before crystallization by vapour diffusion with 6% PEG 6000, 200mM ammonium acetate, 300mM sodium acetate, 50mM HEPES pH7.0 and 5mM TCEP as reservoir solution. Crystals were grown for 5–10 days, cryo-protected in five concentration steps in mother solution supplemented with 22% glycerol, followed by overnight incubation at 8°C before harvesting and freezing in liquid nitrogen. Diffraction data to 3.4Å were collected at 100K at beamline X06SA of the Swiss Light Source. Data were collected at 13.494 KeV, the K-absorption peak of bromine, integrated with XDS/MOSFLM (Kabsch; Leslie, 2006) and the structure solved with molecular replacement using the model of 12-subunit Pol II and PHASER (McCoy et al., 2007). Model building was carried out with COOT (Emsley et al., 2010). Ligand parameterization of the CPD and refinement of modeled co-ordinates was carried out with PHENIX (Adams et al., 2010). The

location of the bromouracil marker nucleotide was determined by calculating an anomalous difference Fourier map using phases from the complete 12-subunit Pol II model.

TEC Assembly and In Vitro Transcription Assays

TECs were assembled on synthetic DNA and RNA oligonucleotides and immobilized on Ni^{2+}-NTA agarose beads (QIAGEN, Valencia, CA) as described previously (Walmacq et al., 2009). Briefly, the 5' radioactively labeled RNA (RNA7 or RNA9) and the template DNA oligonucleotide (TS) containing a single CPD lesion were incubated with the immobilized WT Pol II or Pol II variants, followed by the subsequent addition of the non-template DNA oligonucleotide (NTS) as described (Walmacq et al., 2009). The RNA was extended to the vicinity of the lesion (TEC12) by incubation with NTPs subsets (5 μM, final concentration). *In vitro* transcription assays with lesion-stalled TEC12 were performed as described in the experimental procedures, legends (Fig. 1C, Fig. 3 and Fig. 4) and analyzed as described (Walmacq et al., 2009). Bulk elongation assays in Fig. S1A were done as previously described (Domecq et al., 2010). Briefly, the TECs were assembled on the TS-D111 template and NTS-D111 non-template DNA oligonucleotides with unlabeled 9-nt RNA primer. The RNA in the resulting TEC9 was labeled by incubation with 0.15 μM α-[^{32}P] GTP followed by purification from the unincorporated GTP. The reaction protocol was as shown in Figure S1A.

In Vitro NTP Competition Assays

Fidelity assays were done as shown in Figure S1B and as described in the Supplementary text. Briefly, TECs were assembled by annealing 5'labeled RNA9 oligonucleotide to the template DNA oligonucleotide (TS45) and incubation of Sc RNAP II to the purified RNA-DNA hybrid followed by addition of the non-template DNA strand (NTS45). TEC9 (1-2 nM) was incubated simultaneously with both cognate GTP (20 nM) and non-cognate ATP at increasing concentrations. The reactions were stopped with gel loading buffer after 1 min incubation for the WT Pol II and 30 sec for E1103G mutant before analysis of the RNA products on gel electrophoresis. Accurate GMP incorporation at G10 is discriminated from misincorporation of AMP at A*10 misincoporation by the different mobilities of the short RNAs on gels. The incubation time and ultimately the fraction of chased/unchased TEC9 fractions do not affect the measurements of the fidelity parameter. Note that the incubation time is usually defined adequately to the bulk elongation rate of the Pol II mutants. For instance, the incubation time used for the benchmark E1103G mutant, which increases the bulk elongation rate by 2 to 3-fold, is half the time than the WT in the NTP competition assay.

SUPPLEMENTAL REFERENCES

Adams, P.D., Afonine, P.V., Bunkoczi, G., Chen, V.B., Davis, I.W., Echols, N., Headd, J.J., Hung, L.W., Kapral, G.J., Grosse-Kunstleve, R.W., *et al.* (2010). PHENIX: a comprehensive Python-based system for macromolecular structure solution. Acta Crystallogr D Biol Crystallogr *66*, 213-221.

Armache, K.J., Kettenberger, H., and Cramer, P. (2003). Architecture of initiation-competent 12-subunit RNA polymerase II. Proc Natl Acad Sci U S A *100*, 6964-6968.

Bohr, V.A., Smith, C.A., Okumoto, D.S., and Hanawalt, P.C. (1985). DNA repair in an active gene: removal of pyrimidine dimers from the DHFR gene of CHO cells is much more efficient than in the genome overall. Cell *40*, 359-369.

Brueckner, F., Hennecke, U., Carell, T., and Cramer, P. (2007). CPD damage recognition by transcribing RNA polymerase II. Science *315*, 859-862.

Domecq, C., Kireeva, M., Archambault, J., Kashlev, M., Coulombe, B., and Burton, Z.F. (2010). Site-directed mutagenesis, purification and assay of Saccharomyces cerevisiae RNA polymerase II. Protein Expr Purif *69*, 83-90.

Donahue, B.A., Yin, S., Taylor, J.S., Reines, D., and Hanawalt, P.C. (1994). Transcript cleavage by RNA polymerase II arrested by a cyclobutane pyrimidine dimer in the DNA template. Proc Natl Acad Sci U S A *91*, 8502-8506.

Emsley, P., Lohkamp, B., Scott, W.G., and Cowtan, K. (2010). Features and development of Coot. Acta Crystallogr D Biol Crystallogr *66*, 486-501.

Fousteri, M., and Mullenders, L.H. (2008). Transcription-coupled nucleotide excision repair in mammalian cells: molecular mechanisms and biological effects. Cell Res *18*, 73-84.

Guzder, S.N., Habraken, Y., Sung, P., Prakash, L., and Prakash, S. (1996). RAD26, the yeast homolog of human Cockayne's syndrome group B gene, encodes a DNA-dependent ATPase. J Biol Chem *271*, 18314-18317.

Hanawalt, P.C., and Spivak, G. (2008). Transcription-coupled DNA repair: two decades of progress and surprises. Nat Rev Mol Cell Biol *9*, 958-970.

Haracska, L., Yu, S.L., Johnson, R.E., Prakash, L., and Prakash, S. (2000). Efficient and accurate replication in the presence of 7,8-dihydro-8-oxoguanine by DNA polymerase eta. Nat Genet *25*, 458-461.

Kabsch, W. Xds. Acta Crystallogr D Biol Crystallogr *66*, 125-132.

Kaplan, C.D., Larsson, K.M., and Kornberg, R.D. (2008). The RNA polymerase II trigger loop functions in substrate selection and is directly targeted by alpha-amanitin. Mol Cell *30*, 547-556.

Kettenberger, H., Armache, K.J., and Cramer, P. (2004). Complete RNA polymerase II elongation complex structure and its interactions with NTP and TFIIS. Mol Cell *16*, 955-965.

Kireeva, M., Nedialkov, Y.A., Gong, X.Q., Zhang, C., Xiong, Y., Moon, W., Burton, Z.F., and Kashlev, M. (2009). Millisecond phase kinetic analysis of elongation catalyzed by human, yeast, and Escherichia coli RNA polymerase. Methods *48*, 333-345.

Kireeva, M.L., Domecq, C., Coulombe, B., Burton, Z.F., and Kashlev, M. (2011). Interaction of RNA polymerase II fork loop 2 with downstream non-template DNA regulates transcription elongation. J Biol Chem *286*, 30898-30910.

Kireeva, M.L., Nedialkov, Y.A., Cremona, G.H., Purtov, Y.A., Lubkowska, L., Malagon, F., Burton, Z.F., Strathern, J.N., and Kashlev, M. (2008). Transient reversal of RNA polymerase II active site closing controls fidelity of transcription elongation. Mol Cell *30*, 557-566.

Koyama, H., Ito, T., Nakanishi, T., Kawamura, N., and Sekimizu, K. (2003). Transcription elongation factor S-II maintains transcriptional fidelity and confers oxidative stress resistance. Genes Cells *8*, 779-788.

Koyama, H., Ueda, T., Ito, T., and Sekimizu, K. (2010). Novel RNA polymerase II mutation suppresses transcriptional fidelity and oxidative stress sensitivity in rpb9Delta yeast. Genes Cells *15*, 151-159.

Laine, J.P., and Egly, J.M. (2006). When transcription and repair meet: a complex system. Trends Genet *22*, 430-436.

Lehmann, A.R. (2005). Replication of damaged DNA by translesion synthesis in human cells. FEBS Lett *579*, 873-876.

Leslie, A.G. (2006). The integration of macromolecular diffraction data. Acta Crystallogr D Biol Crystallogr *62*, 48-57.

Li, S., Chen, X., Ruggiero, C., Ding, B., and Smerdon, M.J. (2006). Modulation of Rad26- and Rpb9-mediated DNA repair by different promoter elements. J Biol Chem *281*, 36643-36651.

Li, S., and Smerdon, M.J. (2002). Rpb4 and Rpb9 mediate subpathways of transcription-coupled DNA repair in Saccharomyces cerevisiae. Embo J *21*, 5921-5929.

Malagon, F., Kireeva, M.L., Shafer, B.K., Lubkowska, L., Kashlev, M., and Strathern, J.N. (2006). Mutations in the Saccharomyces cerevisiae RPB1 gene conferring hypersensitivity to 6-azauracil. Genetics *172*, 2201-2209.

Masutani, C., Kusumoto, R., Iwai, S., and Hanaoka, F. (2000). Mechanisms of accurate translesion synthesis by human DNA polymerase eta. Embo J *19*, 3100-3109.

Matsuda, T., Bebenek, K., Masutani, C., Hanaoka, F., and Kunkel, T.A. (2000). Low fidelity DNA synthesis by human DNA polymerase-eta. Nature *404*, 1011-1013.

McCoy, A.J., Grosse-Kunstleve, R.W., Adams, P.D., Winn, M.D., Storoni, L.C., and Read, R.J. (2007). Phaser crystallographic software. J Appl Crystallogr *40*, 658-674.

Mellon, I., Spivak, G., and Hanawalt, P.C. (1987). Selective removal of transcription-blocking DNA damage from the transcribed strand of the mammalian DHFR gene. Cell *51*, 241-249.

Prakash, S., Johnson, R.E., and Prakash, L. (2005). Eukaryotic translesion synthesis DNA polymerases: specificity of structure and function. Annu Rev Biochem *74*, 317-353.

Selby, C.P., Drapkin, R., Reinberg, D., and Sancar, A. (1997). RNA polymerase II stalled at a thymine dimer: footprint and effect on excision repair. Nucleic Acids Res *25*, 787-793.

Svejstrup, J.Q. (2002). Mechanisms of transcription-coupled DNA repair. Nat Rev Mol Cell Biol *3*, 21-29.

Sydow, J.F., Brueckner, F., Cheung, A.C., Damsma, G.E., Dengl, S., Lehmann, E., Vassylyev, D., and Cramer, P. (2009). Structural basis of transcription: mismatch-specific fidelity mechanisms and paused RNA polymerase II with frayed RNA. Mol Cell *34*, 710-721.

Taddei, F., Hayakawa, H., Bouton, M., Cirinesi, A., Matic, I., Sekiguchi, M., and Radman, M. (1997). Counteraction by MutT protein of transcriptional errors caused by oxidative damage. Science *278*, 128-130.

Terleth, C., Schenk, P., Poot, R., Brouwer, J., and van de Putte, P. (1990). Differential repair of UV damage in rad mutants of Saccharomyces cerevisiae: a possible function of G2 arrest upon UV irradiation. Mol Cell Biol *10*, 4678-4684.

Tijsterman, M., and Brouwer, J. (1999). Rad26, the yeast homolog of the cockayne syndrome B gene product, counteracts inhibition of DNA repair due to RNA polymerase II transcription. J Biol Chem *274*, 1199-1202.

Tijsterman, M., Verhage, R.A., van de Putte, P., Tasseron-de Jong, J.G., and Brouwer, J. (1997). Transitions in the coupling of transcription and nucleotide excision repair within RNA polymerase II-transcribed genes of Saccharomyces cerevisiae. Proc Natl Acad Sci U S A *94*, 8027-8032.

Tornaletti, S., Donahue, B.A., Reines, D., and Hanawalt, P.C. (1997). Nucleotide sequence context effect of a cyclobutane pyrimidine dimer upon RNA polymerase II transcription. J Biol Chem *272*, 31719-31724.

Tornaletti, S., Park-Snyder, S., and Hanawalt, P.C. (2008). G4-forming sequences in the non-transcribed DNA strand pose blocks to T7 RNA polymerase and mammalian RNA polymerase II. J Biol Chem *283*, 12756-12762.

Tornaletti, S., Patrick, S.M., Turchi, J.J., and Hanawalt, P.C. (2003). Behavior of T7 RNA polymerase and mammalian RNA polymerase II at site-specific cisplatin adducts in the template DNA. J Biol Chem *278*, 35791-35797.

Tornaletti, S., Reines, D., and Hanawalt, P.C. (1999). Structural characterization of RNA polymerase II complexes arrested by a cyclobutane pyrimidine dimer in the transcribed strand of template DNA. J Biol Chem *274*, 24124-24130.

Troelstra, C., van Gool, A., de Wit, J., Vermeulen, W., Bootsma, D., and Hoeijmakers, J.H. (1992). ERCC6, a member of a subfamily of putative helicases, is involved in Cockayne's syndrome and preferential repair of active genes. Cell *71*, 939-953.

van Gool, A.J., Verhage, R., Swagemakers, S.M., van de Putte, P., Brouwer, J., Troelstra, C., Bootsma, D., and Hoeijmakers, J.H. (1994). RAD26, the functional S. cerevisiae homolog of the Cockayne syndrome B gene ERCC6. Embo J *13*, 5361-5369.

Vassylyev, D.G., Vassylyeva, M.N., Zhang, J., Palangat, M., Artsimovitch, I., and Landick, R. (2007). Structural basis for substrate loading in bacterial RNA polymerase. Nature *448*, 163-168.

Venema, J., Mullenders, L.H., Natarajan, A.T., van Zeeland, A.A., and Mayne, L.V. (1990). The genetic defect in Cockayne syndrome is associated with a defect in repair of UV-induced DNA damage in transcriptionally active DNA. Proc Natl Acad Sci U S A *87*, 4707-4711.

Verhage, R., Zeeman, A.M., de Groot, N., Gleig, F., Bang, D.D., van de Putte, P., and Brouwer, J. (1994). The RAD7 and RAD16 genes, which are essential for pyrimidine dimer removal from the silent mating type loci, are also required for repair of the nontranscribed strand of an active gene in Saccharomyces cerevisiae. Mol Cell Biol *14*, 6135-6142.

Verhage, R.A., van Gool, A.J., de Groot, N., Hoeijmakers, J.H., van de Putte, P., and Brouwer, J. (1996). Double mutants of Saccharomyces cerevisiae with alterations in global genome and transcription-coupled repair. Mol Cell Biol *16*, 496-502.

Walmacq, C., Kireeva, M.L., Irvin, J., Nedialkov, Y., Lubkowska, L., Malagon, F., Strathern, J.N., and Kashlev, M. (2009). Rpb9 subunit controls transcription fidelity by delaying NTP sequestration in RNA polymerase II. J Biol Chem *284*, 19601-19612.

Wang, D., Bushnell, D.A., Westover, K.D., Kaplan, C.D., and Kornberg, R.D. (2006). Structural basis of transcription: role of the trigger loop in substrate specificity and catalysis. Cell *127*, 941-954.

Waters, L.S., Minesinger, B.K., Wiltrout, M.E., D'Souza, S., Woodruff, R.V., and Walker, G.C. (2009). Eukaryotic translesion polymerases and their roles and regulation in DNA damage tolerance. Microbiol Mol Biol Rev *73*, 134-154.

Xiong, Y., and Burton, Z.F. (2007). A tunable ratchet driving human RNA polymerase II translocation adjusted by accurately templated nucleoside triphosphates loaded at downstream sites and by elongation factors. J Biol Chem *282*, 36582-36592.

Yang, W., and Woodgate, R. (2007). What a difference a decade makes: insights into translesion DNA synthesis. Proc Natl Acad Sci U S A *104*, 15591-15598.